Available online at www.sciencedirect.com
SCIENCE DIRECT
Comput. Methods Appl. Mech. Engrg. 195 (2006) 5582–5596
Computer methods in applied mechanics and engineering
www.elsevier.com/locate/cma

Long-term behavior of polynomial chaos in stochastic flow simulations

Xiaoliang Wan, George Em Karniadakis *

Division of Applied Mathematics, Center for Fluid Mechanics, Brown University, Box 1966, 37 Manning Street, Providence, RI 02912, USA

Received 2 August 2005; received in revised form 17 October 2005; accepted 18 October 2005

Abstract

In this paper we focus on the long-term behavior of generalized polynomial chaos (gPC) and multi-element generalized polynomial chaos (ME-gPC) for partial differential equations with stochastic coefficients. First, we consider the one-dimensional advection equation with a uniform random transport velocity and derive error estimates for gPC and ME-gPC discretizations. Subsequently, we extend these results to other random distributions and high-dimensional random inputs with numerical verification using the algebraic convergence rate of ME-gPC. Finally, we apply our results to *noisy* flow past a stationary circular cylinder. Simulation results demonstrate that ME-gPC is effective in improving the accuracy of gPC for a long-term integration whereas high-order gPC cannot capture the correct asymptotic behavior.

Keywords: Polynomial chaos; Uncertainty; Differential equation

1. Introduction

Polynomial chaos (PC) has been used extensively in the last decade to model uncertainty in physical applications [1–6]. It is based on the original ideas of *homogenous chaos* (*Wiener-chaos*) first formulated by Wiener as the span of Hermite polynomial functionals of a Gaussian process [7]. Ghanem and Spanos were the first to combine Wiener-chaos with a finite element method to model uncertainty addressing solid mechanics applications [1,8,9]. A more general framework, termed *generalized polynomial chaos* (gPC), was proposed in [10] by Xiu and Karniadakis, following the framework of Ghanem and Spanos, based on the *correspondence* between the PDFs of certain random variables and the weight functions of orthogonal polynomials of the Askey scheme. The family of gPC includes Hermite-chaos as a subset and provides optimal bases for stochastic processes represented by random variables of commonly used distributions, such as uniform distribution, Beta distribution, etc. Polynomial chaos was combined with wavelets in [11,12] to deal with discontinuities for uniform random inputs for which standard PC or gPC fails to converge. To solve differential equations with stochastic inputs following the procedure established by Ghanem and Spanos, the random solution is expanded spectrally by polynomial chaos and a Galerkin projection scheme is subsequently used to transform the original stochastic problem into a deterministic one with a large dimensional parameter [1,10,6].

On the other hand, Deb et al. [13] have proposed to employ finite elements in the random space to approximate the stochastic dependence of the solution. This approach also reduces a stochastic differential equation to a high dimensional *deterministic* one. This method was later studied theoretically within the framework of deterministic finite element method in [14]. Since a finite element method is generally used to solve the obtained deterministic PDE system, the above methods are called *stochastic Galerkin finite element method* in [14] while the scheme in [1,10] is classified as $p \times h$ version and the

* Corresponding author. Tel.: +1 401 863 1217; fax: +1 401 863 3369.
E-mail address: gk@dam.brown.edu (G.E. Karniadakis).

0045-7825/$ - see front matter © 2005 Elsevier B.V. All rights reserved.
doi:10.1016/j.cma.2005.10.016

scheme in [13] as $k \times h$ version. Here p denotes the polynomial order of polynomial chaos, k the element size in the random space, and h the element size in the physical space. Both schemes use finite elements in the physical space. The $p \times h$ version relies on the global representation in the entire random space by polynomial chaos while the $k \times h$ version is based on the discretization of the random space using the same basis as the deterministic finite element method to approximate the random field locally. Both concepts and the terminology introduced here have similarities with the spectral/*hp* element method for deterministic problems [15,16].

Although gPC works effectively for many problems, e.g., elliptic and parabolic PDEs with stochastic coefficients [14,6], it cannot deal with some other differential equations, e.g., the Kraichnan–Orszag's three-mode ODE system for modeling turbulence [17] or the Navier–Stokes equations for unsteady noisy flows such as flow past a stationary cylinder [18]. For these problems gPC fails to converge after a short time, and increasing the polynomial order helps little for the convergence. There exist at least two reasons for the divergence of gPC:

(1) singularity in the random space, and
(2) long-term integration.

The former was studied in [11,12] with Wiener–Haar expansions and in [19,20] with ME-gPC. In this work, we focus on the second one: long-term integration. In particular, we are interested in the cases which are related to *random frequencies*. We use a simple one-dimensional advection equation with a uniform random transport velocity as a model problem. We first derive the error estimates of gPC and ME-gPC for the Legendre-chaos expansion. Based on these error estimates we obtain a relation between gPC and ME-gPC, which we verify by numerical computations. We subsequently generalize such a relation to other random distributions and more general random inputs. Lastly, we consider a physical problem: noisy flow past a stationary circular cylinder, where we use the obtained results to analyze the convergence of gPC and ME-gPC.

This paper is structured as follows. In Section 2 we present an overview of gPC and ME-gPC. In Section 3 we study theoretically the one-dimensional stochastic advection equation. In Section 4 we present results for stochastic simulations of noisy flow past a stationary circular cylinder. We conclude with a short discussion in Section 5.

2. Overview of gPC and ME-gPC

Let $(\Omega, \mathscr{F}, P)$ be a complete probability space, where Ω is the sample space, $\mathscr{F}$ is the σ-algebra of subsets of Ω and P is a probability measure. An $\mathbb{R}^d$-valued random variable is defined as

$$\boldsymbol{Y} = (Y_1(\omega), \ldots, Y_d(\omega)) : (\Omega, \mathscr{F}) \mapsto (\mathbb{R}^d, \mathscr{B}^d), \tag{1}$$

where $d \in \mathbb{N}$ and $\mathscr{B}^d$ is the σ-algebra of Borel subsets of $\mathbb{R}^d$. If uncertainty is included in the PDEs, the solutions can be referred to as a random field $\mathbf{u}(\mathbf{x}, t; \omega)$, where $\mathbf{x}$ denotes the physical space and t the time. For any fixed $\mathbf{x}$ and t, $\mathbf{u}(\mathbf{x}, t; \omega)$ is a $\mathbb{R}^{d_\mathrm{p}}$-valued random variable, where d_p is the dimension of physical domain ($d_\mathrm{p} \leqslant 3$). We generally assume that $\mathbf{u}(\mathbf{x}, t; \omega)$ is a *second-order* random field denoted as $\mathbf{u}(\mathbf{x}, t; \omega) \in L_2(\Omega, \mathscr{F}, P)$, where

$$\int_\Omega \mathbf{u}^2(\mathbf{x}, t; \omega)\, \mathrm{d}P(\omega) < \infty. \tag{2}$$

We expect that all viscous flows satisfy this constraint.

2.1. Generalized polynomial chaos (gPC)

Generalized polynomial chaos is a spectral polynomial expansion for a second-order random field $\mathbf{u}(\mathbf{x}, t; \omega)$, i.e.,

$$\mathbf{u}(\mathbf{x}, t; \omega) = \sum_{i=0}^{\infty} \hat{a}_i(\mathbf{x}, t) \Phi_i(\boldsymbol{Y}(\omega)), \tag{3}$$

where $\{\Phi_i(\boldsymbol{Y})\}$ denote the basis of gPC in terms of $\boldsymbol{Y}$; this spectral expansion converges in the L_2 sense. We usually select a weighted orthogonal system $\{\Phi_i(\boldsymbol{Y})\}$ in $L_2(\Omega, \mathscr{F}, P)$ satisfying the orthogonality relation

$$\langle \Phi_i \Phi_j \rangle = \langle \Phi_i^2 \rangle \delta_{ij}, \tag{4}$$

where δ_{ij} is the Kronecker delta, and $\langle \cdot, \cdot \rangle$ denotes the ensemble average with respect to the probability measure P. The index in Eq. (3) and $d \in \mathbb{N}$ are, in general, infinite. In practice, both limits will be truncated at a certain level.

For a certain $\mathbb{R}^d$-valued random variable $\boldsymbol{Y}$, the gPC basis $\{\Phi_i\}$ can be chosen in such a way that its weight function has the same form as the probability density function (PDF) of $\boldsymbol{Y}$. The corresponding type of classical orthogonal polynomials $\{\Phi_i\}$ and their associated random variable $\boldsymbol{Y}$ are listed in Table 1 [10]. For *arbitrary* probability measures, the orthogonality must be maintained numerically, as we explain in the next subsection.

Table 1
Correspondence of the type of Wiener–Askey polynomial chaos and their underlying random variables

Random variables $\boldsymbol{Y}$	Wiener–Askey chaos $\{\Phi_i(\boldsymbol{Y})\}$	Support
Continuous		
Gaussian	Hermite-chaos	$(-\infty,\infty)$
Gamma	Laguerre-chaos	$[0,\infty)$
Beta	Jacobi-chaos	$[a,b]$
Uniform	Legendre-chaos	$[a,b]$
Discrete		
Poisson	Charlier-chaos	$\{0,1,2,\ldots\}$
Binomial	Krawtchouk-chaos	$\{0,1,\ldots,N\}$
Negative binomial	Meixner-chaos	$\{0,1,2,\ldots\}$
Hypergeometric	Hahn-chaos	$\{0,1,\ldots,N\}$

$N \geqslant 0$ is a finite integer.

2.2. Multi-element generalized polynomial chaos (ME-gPC)

We assume that $\boldsymbol{Y}$ is defined on $B = \times_{i=1}^{d}[a_i, b_i]$, where a_i and b_i are finite or infinite in $\mathbb{R}$ and the components of $\boldsymbol{Y}$ are *independent identically-distributed (i.i.d.)* random variables. We define a decomposition $\mathbf{D}$ of B as

$$\mathbf{D} = \begin{cases} B_k = [a_{k,1}, b_{k,1}) \times [a_{k,2}, b_{k,2}) \times \cdots \times [a_{k,d}, b_{k,d}], \\ B = \bigcup\limits_{k=1}^{N} B_k, \\ B_{k_1} \cap B_{k_2} = \emptyset \quad \text{if } k_1 \neq k_2, \end{cases} \tag{5}$$

where $k, k_1, k_2 = 1, 2, \ldots, N$. Based on the decomposition $\mathbf{D}$, we define the following indicator random variables

$$I_{B_k} = \begin{cases} 1 & \text{if } \boldsymbol{Y} \in B_k, \\ 0 & \text{otherwise.} \end{cases} \tag{6}$$

Thus, $\Omega = \bigcup_{k=1}^{N} I_{B_k}^{-1}(1)$ is a decomposition of the sample space Ω, where

$$I_{B_i}^{-1}(1) \cap I_{B_j}^{-1}(1) = \emptyset \quad \text{for } i \neq j. \tag{7}$$

Subsequently, we define a new $\mathbb{R}^d$-valued random variables $\boldsymbol{\zeta}_k : I_{B_k}^{-1}(1) \mapsto B_k$ on the probability space $(I_{B_k}^{-1}(1), \mathscr{F} \cap I_{B_k}^{-1}(1), P(\cdot | I_{B_k} = 1))$ subject to a conditional PDF

$$f_k(\boldsymbol{y} | I_{B_k} = 1) = \frac{f(\boldsymbol{y})}{\Pr(I_{B_k} = 1)}, \tag{8}$$

where $f(\boldsymbol{y})$ denotes the PDF of $\boldsymbol{Y}$ and $\Pr(I_{B_k} = 1) > 0$. In practice, we usually map $\boldsymbol{\zeta}_k$ to a new random variable $\boldsymbol{Y}_k$ defined on $[-1, 1]^d$ to avoid numerical overflow in computer [20], using the following linear transform

$$\zeta_{k,i} = g(Y_{k,i}) : \zeta_{k,i} = \frac{b_{k,i} - a_{k,i}}{2} Y_{k,i} + \frac{b_{k,i} + a_{k,i}}{2}, \tag{9}$$

where $i = 1, 2, \ldots, d$ and $k = 1, 2, \ldots, N$. To this end, we present a decomposition of random space, which is very similar with the decomposition of physical space using separable elements.

Based on the random variables $\{\boldsymbol{Y}_k\}$, a scheme, called *multi-element* generalized polynomial chaos (ME-gPC), was proposed in [19,20]. Based on ME-gPC, $\mathbf{u}(\mathbf{x}, t; \omega)$ can be expressed as [19]

$$\mathbf{u}(\mathbf{x}, t; \omega) = \sum_{k=1}^{N} \sum_{i=0}^{M} \hat{a}_{k,i}(\mathbf{x}, t) \Phi_{k,i}(\boldsymbol{Y}_k(\boldsymbol{Y})) I_{B_k}, \tag{10}$$

where $\{\Phi_{k,i}\}$ is the local chaos basis in element k and M is the number of chaos modes. The key idea of ME-gPC is to implement gPC element-by-element when the global spectral expansion is not efficient to capture the random behavior. Thus, the basic procedure of ME-gPC is quite similar with the deterministic spectral element method. In the decomposition of physical space using continuous Galerkin projections, we need to treat carefully the connectivity (C^0 continuity) between two adjacent elements; however, in the decomposition of random space the following C^0-type continuity

$$\mathbf{u}_{B_1}(\boldsymbol{Y}) = \mathbf{u}_{B_2}(\boldsymbol{Y}), \quad \boldsymbol{Y} \in \overline{B}_1 \cap \overline{B}_2, \tag{11}$$

where $\overline{B}_i$ is the closure of element B_i, is not required since the Lebesgue measure of the interface between two random elements is zero and most statistics we are interested in are defined as a Lebesgue integration.

In the decomposition of random space, the PDF of $\boldsymbol{Y}$ is decomposed simultaneously, which implies that the original gPC basis will, in general, lose local orthogonality in random elements. The only exception is the Legendre-chaos for the uniform distribution [19]. For other distributions, orthogonal polynomials with respect to the PDF of local random variable $\boldsymbol{Y}_k$ can be constructed numerically. Given an *arbitrary* PDF, the Stieltjes procedure and the Lanczos algorithm [21] can be used to construct the following orthogonal system

$$\begin{aligned} &\pi_{i+1}(t) = (t-\alpha_i)\pi_i(t) - \beta_i\pi_{i-1}(t), \quad i = 0,1,\ldots, \\ &\pi_0(t) = 1, \qquad \pi_{-1}(t) = 0, \end{aligned} \tag{12}$$

where $\{\pi_i(t)\}$ is a set of (monic) orthogonal polynomials,

$$\pi_i(t) = t^i + \text{lower-degree terms}, \quad i = 0,1,\ldots \tag{13}$$

and the coefficients α_i and β_i are uniquely determined by a positive (probability) measure. The orthogonal system $\{\pi_i(\boldsymbol{Y}_k)\}$ will serve as a local gPC basis.

In ME-gPC, relative low polynomial orders (5–8) are preferred locally; thus, the numerical re-construction can be implemented efficiently and accurately [20]. Numerical experiments show that the cost of maintaining local orthogonality is negligible compared to the cost of a standard Galerkin gPC solver.

3. Long-term integration of gPC and ME-gPC

In this section we study the long-term behavior of gPC and ME-gPC analytically using the following one-dimensional stochastic advection equation

$$\frac{\partial u}{\partial t} + V(\xi)\frac{\partial u}{\partial x} = 0 \tag{14}$$

subject to the initial condition

$$u(x) = u_0(x;\xi), \tag{15}$$

where ξ is a one-dimensional uniform random variable defined on $[-1,1]$ and $V(\xi) \in L_2(\Omega,\mathscr{F},P)$. In particular, we assume that

$$V(\xi) = \bar{v} + \sigma\xi, \qquad u_0(x;\xi) = \sin n\pi(1+x), \quad x \in [-1,1], \tag{16}$$

where σ is a constant, $\bar{v}$ is the mean of transport velocity and $n \in \mathbb{N}$. It is easy to obtain the exact solution for this case as

$$u(x,t;\xi) = \sin n\pi(1+x-(\bar{v}+\sigma\xi)t), \tag{17}$$

which shows that the frequency of this stochastic process is random.

3.1. Error estimates for gPC

Let $\{P_i(\xi)\}$ denote the orthogonal basis of Legendre-chaos and $\mathscr{P}_M$ denote the projection operator as

$$\mathscr{P}_M u(x,t;\xi) = \sum_{i=0}^{M} u_i(x,t)P_i(\xi), \tag{18}$$

where

$$u_i(x,t) = \frac{1}{\langle P_i^2(\xi)\rangle}\int_{-1}^{1} u(x,t;\xi)P_i(\xi)\frac{1}{2}\mathrm{d}\xi. \tag{19}$$

We study the convergence of $\mathscr{P}_M u(x,t;\xi)$ since it can demonstrate the main properties of numerical convergence.

Theorem 1. *Let ϵ_M denote the error of the second-order moment of $\mathscr{P}_M u$. Given time t and polynomial order M, ϵ_M can be bounded as*

$$\epsilon_M \leqslant C(M)\frac{q_M^{2M+2}}{1-q_M^2}, \tag{20}$$

where $C(M)$ is a constant depending on M and

$$q_M = \frac{\sigma n\pi \mathrm{e} t}{2M+2} < 1. \tag{21}$$

Here e *is the base of natural logarithm.*

Proof. According to the following formula in [22]

$$\sin c\pi(z+a) = \frac{1}{\sqrt{2c}} \sum_{i=0}^{\infty} (2i+1) J_{i+1/2}(c\pi) \sin\left(c\pi a + \frac{1}{2} i\pi\right) P_i(z), \tag{22}$$

we obtain the polynomial chaos expansion of the exact solution (17) as

$$u = -\frac{1}{\sqrt{2n\sigma t}} \sum_{i=0}^{\infty} (2i+1) J_{i+1/2}(\sigma n\pi t) \sin\left(n\pi(\bar{v}t - x - 1) + \frac{1}{2} i\pi\right) P_i(\xi), \tag{23}$$

where $J_{i+1/2}$ are Bessel functions of the first kind. Using the orthogonality of Legendre polynomials, we obtain

$$\langle u^2(x,t;\xi)\rangle = \frac{1}{2n\sigma t} \sum_{i=0}^{\infty} (2i+1) J_{i+1/2}^2(\sigma n\pi t) \sin^2\left(n\pi(\bar{v}t - x - 1) + \frac{1}{2} i\pi\right), \tag{24}$$

where $\langle P_i(\xi) P_j(\xi)\rangle = \delta_{ij}/(2i+1)$ is employed. Then ϵ_M can be expressed as

$$\epsilon_M \equiv \langle u^2\rangle - \langle (\mathscr{P}_M u)^2\rangle = \frac{1}{2n\sigma t} \sum_{i=M+1}^{\infty} (2i+1) J_{i+1/2}^2(\sigma n\pi t) \sin^2\left(n\pi(\bar{v}t - x - 1) + \frac{1}{2} i\pi\right). \tag{25}$$

It is known (see [23]) that

$$\sqrt{\frac{\pi}{2\sigma n\pi t}} J_{i+1/2}(\sigma n\pi t) = \frac{(\sigma n\pi t)^i}{2^{i+1} i!} \int_0^{\pi} \cos((\sigma n\pi t)\cos(\theta)) \sin^{2i+1}\theta \, \mathrm{d}\theta. \tag{26}$$

By substituting Eq. (26) into Eq. (25), ϵ_M can be approximated as

$$\epsilon_M = \sum_{i=M+1}^{\infty} \frac{(2i+1)(\sigma n\pi t)^{2i}}{2^{2i+2}(i!)^2} A_i \sin^2\left(n\pi(\bar{v}t - x - 1) + \frac{1}{2} i\pi\right),$$

where

$$A_i = \left(\int_0^{\pi} \cos(\sigma n\pi t \cos(\theta)) \sin^{2i+1}\theta \, \mathrm{d}\theta\right)^2.$$

Using Stirling's formula [23] for the factorial $i!$, we obtain that

$$\epsilon_M \approx \sum_{i=M+1}^{\infty} \frac{(2i+1)(\sigma n\pi t \mathrm{e})^{2i}}{8\pi i (2i)^{2i}} A_i \sin^2\left(n\pi(\bar{v}t - x - 1) + \frac{1}{2} i\pi\right),$$

where e is the base of natural logarithm. For a fixed time t, the error ϵ_M can be bounded as

$$\epsilon_M \leqslant C_1 \sum_{i=M+1}^{\infty} \frac{(2M+3)(\sigma n\pi \mathrm{e} t)^{2i}}{8\pi(M+1)(2M+2)^{2i}} = C_1 \frac{(2M+3) q_M^{2M+2}}{8\pi(M+1)(1-q_M^2)},$$

where C_1 is a constant and $q_M = \sigma n\pi \mathrm{e} t/(2M+2)$. Here the condition $q_M < 1$ is assumed for the convergence of summation. We subsequently check the constant C_1. Since $\sin\theta \geqslant 0$ in $\theta \in [0,\pi]$, we obtain that

$$A_i^{1/2} \leqslant \int_0^{\pi} \sin^{2i+1}\theta \, \mathrm{d}\theta.$$

Let $B_i = \int_0^{\pi} \sin^{2i+1}\theta \, \mathrm{d}\theta$. Using $\sin^2\theta + \cos^2\theta = 1$, the following relationship can be obtained

$$B_i = \int_0^{\pi} \sin^{2i-1}\theta \, \mathrm{d}\theta - \int_0^{\pi} \sin^{2i-1}\theta \cos^2\theta \, \mathrm{d}\theta = B_{i-1} - \int_0^{\pi} \sin^{2i-1}\theta \cos^2\theta \, \mathrm{d}\theta.$$

Since the second term on the right-hand side is positive, we know that the sequence $\{B_i\}$ is decreasing. Thus, we can bound A_i as

$$A_i \leqslant B_i^2 \leqslant B_{M+1}^2, \quad i \geqslant (M+1).$$

Let $C_1 = B_{M+1}^2$ and $C(M) = C_1(2M+3)/8\pi(M+1)$, then the conclusion follows immediately. □

In Theorem 1, $q_M < 1$ is assumed for the convergence of summation in ϵ_M. For a general case we have the following corollary:

Corollary 2. *Given time t and polynomial order M, ϵ_M can be bounded as*

$$\epsilon_M \leqslant \frac{1}{2\sigma t}\sum_{i=M+1}^{\hat{M}}(2i+1)J_{i+1/2}^2(\sigma n\pi t) + C(\widehat{M})\frac{q_{\hat{M}}^{2\hat{M}+2}}{1-q_{\hat{M}}^2}, \tag{27}$$

where $q_{\hat{M}}$ is a function of $\widehat{M}$ defined as in Eq. (21) and $q_{\hat{M}} < 1$.

3.2. Error estimates for ME-gPC

Let $\widehat{\mathscr{P}}_M$ denote the projection of $u(x,t;\xi)$ onto the basis of ME-gPC.

Theorem 3. *Given a decomposition of random space of ξ with element length $L_k = b_k - a_k$, $k = 1,2,\ldots,N$, the error $\hat{\epsilon}_M$ of the second-order moment of $\widehat{\mathscr{P}}_M u$ can be bounded as*

$$\hat{\epsilon}_M \leqslant C(M)\sum_{k=1}^{N}\frac{q_{k,M}^{2M+2}}{1-q_{k,M}^2}\Pr(I_{B_k}=1), \tag{28}$$

where $C(M)$ is a constant depending on M and

$$q_{k,M} = \frac{\sigma n\pi \mathrm{e} L_k t}{2(2M+2)} < 1. \tag{29}$$

Proof. According to Eq. (10), we know that $\widehat{\mathscr{P}}_M$ can be expressed as

$$\widehat{\mathscr{P}}_M = \sum_{k=1}^{N}\widehat{\mathscr{P}}_{k,M} I_{B_k}, \tag{30}$$

where $\widehat{\mathscr{P}}_{k,M}$ is a local projection operator defined as

$$\widehat{\mathscr{P}}_{k,M}u(x,t;\xi) = \mathscr{P}_M u\left(x,t;\frac{b_k-a_k}{2}\xi + \frac{b_k+a_k}{2}\right). \tag{31}$$

Then, the second-order moment can be expressed as

$$\langle(\widehat{\mathscr{P}}_M u(x,t;\xi))^2\rangle = \left\langle\left(\sum_{k=1}^{N}\widehat{\mathscr{P}}_{k,M}u(x,t;\xi)I_{B_k}\right)^2\right\rangle = \sum_{k=1}^{N}\langle(\widehat{\mathscr{P}}_{k,M}u(x,t;\xi))^2\rangle\Pr(I_{B_k}=1). \tag{32}$$

Thus, $\hat{\epsilon}_M$ takes the following form

$$\hat{\epsilon}_M = \sum_{k=1}^{N}\hat{\epsilon}_{k,M}\Pr(I_{B_k}=1), \tag{33}$$

where $\hat{\epsilon}_{k,M}$ is the error of the second-order moment of $\widehat{\mathscr{P}}_{k,M}u(x,t;\xi)$. We now check the behavior of $\hat{\epsilon}_{k,M}$. Given a random element $B_k = [a_k, b_k]$, the local problem in ME-gPC is to find the solution of the following transformed equation

$$\frac{\partial u}{\partial t} + \left(\bar{v} + \sigma\left(\frac{b_k-a_k}{2}\xi_k + \frac{b_k+a_k}{2}\right)\right)\frac{\partial u}{\partial x} = 0,$$

where ξ_k is the local uniform random variable defined on $[-1,1]$. The exact solution of above equation is

$$u(x,t;\xi_k) = \sin n\pi\left[1 + x - \left(\bar{v} + \sigma\left(\frac{b_k-a_k}{2}\xi_k + \frac{b_k+a_k}{2}\right)\right)t\right].$$

Using a similar procedure as in Section 3.1, we can bound $\hat{\epsilon}_{k,M}$ as

$$\hat{\epsilon}_{k,M} \leqslant \frac{C(M)q_{k,M}^{2M+2}}{1-q_{k,M}^2},$$

where

$$q_{k,M} = \frac{\sigma n\pi \mathrm{e}(b_k-a_k)t}{2(2M+2)} < 1.$$

Using Eq. (33), the conclusion follows immediately. □

3.3. Relation between ϵ_M and $\hat{\epsilon}_M$

From Theorem 1, we can see that q_M increases *linearly* in terms of time t, which implies that gPC will lose p-convergence after a finite time. To keep a certain accuracy, the polynomial order of gPC must increase with time. Let

$$\delta = \frac{C(M)}{1-q_M^2} q_M^{2M+2}, \tag{34}$$

where δ denotes a desired accuracy. By solving such an equation we obtain that

$$t = \frac{1}{\sigma n \pi \mathrm{e}} \left(\frac{\delta(1-q_M^2)}{C(M)} \right)^{1/(2M+2)} (2M+2). \tag{35}$$

Since $[\delta(1-q_M^2)/C(M)]^{1/(2M+2)} \to 1$ when $M \to \infty$, we obtain that

$$t \approx \frac{2M+2}{\sigma n \pi \mathrm{e}}, \tag{36}$$

which is a linear relation. It is instructive to define the increasing speed of polynomial order as

$$\frac{\mathrm{d}M}{\mathrm{d}t} \approx \frac{\sigma n \pi \mathrm{e}}{2}, \tag{37}$$

which shows that to maintain an accuracy δ the polynomial order must increase at a speed $\sigma n \pi \mathrm{e}/2$; we note that $n/2$ is the wave number in the initial condition. We can see that the speed is proportional to the wave number and the degree of perturbation, which implies that gPC will quickly fail to converge for a problem with a large perturbation or wave number if a random frequency in time is involved.

Theorem 4. *To maintain a certain accuracy of the second-order moment of $\mathscr{P}_M u$, the polynomial order of gPC must increase with time and the following relation is satisfied*

$$M \approx \tfrac{1}{2}\sigma n \pi \mathrm{e} t - 1. \tag{38}$$

We assume that a uniform mesh is employed and p-convergence is maintained, in other words, $q_M < 1$ and $q_{k,M} < 1$ with $k = 1, 2, \ldots, N$. Thus, we have

$$\hat{\epsilon}_M = C(M) \frac{\hat{q}_M^{2M+2}}{1-\hat{q}_M^2}. \tag{39}$$

The ratio of $\hat{\epsilon}_M$ and ϵ_M, for a fixed time t and polynomial order M, is

$$\frac{\hat{\epsilon}_M}{\epsilon_M} = \left(\frac{1}{N}\right)^{2M+2} \frac{1-q_M^2}{1-(\frac{1}{N})^2 q_M^2} \sim \left(\frac{1}{N}\right)^{2M+2}, \tag{40}$$

which is consistent with the k-convergence ($\epsilon \propto N^{-2(M+1)}$) of ME-gPC (see [13,14,19,20]). Let us consider that gPC and ME-gPC of polynomial order M reach accuracy of the same order. To satisfy this, we need to have

$$q_M = \hat{q}_M, \tag{41}$$

which yields

$$\hat{t}_M = N t_M, \tag{42}$$

where $\hat{t}_M$ and t_M denote time for ME-gPC and gPC, respectively.

Theorem 5. *Suppose that the error, ϵ, of the second-order moment of gPC of order M is maintained in the range $t \leqslant t_g$. Based on a uniform mesh with N random elements, ME-gPC of order M can maintain the accuracy $\mathrm{O}(\epsilon)$ in the range $t \leqslant N t_g$. In other words, ME-gPC can extend the valid integration time of gPC linearly by a factor N.*

If the mesh is non-uniform, the aforementioned linearity is still valid; however, the factor will be less than N. We assume that $\bigcup_{k=1}^{N} B_k$ is a decomposition for ξ of uniform distribution and the length of B_k is an increasing series, $0 < l_{B_1} \leqslant l_{B_2} \leqslant \cdots \leqslant l_{B_N}$. From the proof of Theorem 3, we know that

$$\hat{\epsilon}_M = \sum_{k=1}^{N} \hat{\epsilon}_{k,M} \Pr(I_{B_k} = 1) \leqslant C(M) \sum_{k=1}^{N} \frac{q_{k,M}^{2M+2}}{1-q_{k,M}^2} \frac{l_{B_k}}{2}, \tag{43}$$

where

$$q_{k,M} = \frac{\sigma n \pi e l_{B_k} t}{2(2M+2)} \quad \text{and} \quad \Pr(I_{B_k} = 1) = \frac{l_{B_k}}{2}.$$

We define a function

$$Q(z) = \frac{q_z^{2M+2}}{1-q_z^2},$$

where

$$q_z = \frac{\sigma n \pi e t}{(2M+2)} z.$$

It is easy to verify that $Q(z)$ is an increasing function with respect to z. Let $z_k = l_{B_k}/2$. We can obtain

$$Q(z_1) = \sum_{k=1}^{N} Q(z_1) z_k \leqslant \sum_{k=1}^{N} Q(z_k) z_k \leqslant \sum_{k=1}^{N} Q(z_N) z_k = Q(z_N),$$

where

$$\sum_{k=1}^{N} z_k = 1, \quad 0 < z_1 \leqslant z_2 \leqslant \cdots \leqslant z_N.$$

To satisfy $\epsilon_M = \hat{\epsilon}_M$, we need

$$Q(z_1) \leqslant Q(1) \leqslant Q(z_N),$$

which implies that

$$\frac{2}{l_{B_N}} t_M \leqslant \hat{t}_M \leqslant \frac{2}{l_{B_1}} t_M. \tag{44}$$

3.4. Other distributions and high-dimensional random inputs

In ME-gPC, the PDF of ξ will be decomposed simultaneously with the random space; thus, the local orthogonality has to be maintained numerically. The only exception is the Legendre-chaos [19] due to the nice properties of uniform distribution. It is, in general, difficult to analyze theoretically the convergence for the numerical basis of ME-gPC. In this work, we compare the performance of gPC and ME-gPC numerically for other distributions.

The k-type convergence was shown theoretically in [14,13] to be

$$\|\mathbb{E}[u] - \mathbb{E}[u_M]\|_{L_2(D)} \leqslant Ck^{2(M+1)}, \qquad \|\mathbb{E}[u^2] - \mathbb{E}[u_M^2]\|_{L_2(D)} \leqslant Ck^{2(M+1)} \tag{45}$$

using an stochastic elliptic model problem, where C is a constant depending on M, and k denotes the maximum size of random elements. We note here that D indicates the physical space. It was shown in [19,20] that the index of algebraic convergence of ME-gPC for the mean and variance goes asymptotically to $2(M+1)$ for a uniform mesh, which is consistent with Eq. (45). Note that the error bound (45) is independent of probability measures. Such observations imply that for any probability measure the following relation (see Eq. (40))

$$\frac{\hat{\epsilon}_M}{\epsilon_M} \sim C(M) \left(\frac{\hat{t}_M}{N t_M} \right)^{2M+2} \tag{46}$$

holds for the solution of Eq. (17), where the constant C depends on the polynomial order M. Here we include the time t together with the number N of random elements because in the kth random element of ME-gPC the solution takes the form

$$u(x,t;\xi_k) = \sin n\pi \left(1 + x - \left(\bar{v}_k + \frac{\sigma t}{N} \xi_k \right) \right), \tag{47}$$

where t and N can be treated together. From Eq. (46) we can see that if we re-scale the time of gPC by the number N, $\hat{\epsilon}_M/\epsilon_M$ will be a constant depending on the polynomial order. However, such a relation will be reached asymptotically because of the non-uniform random distribution [20].

It is easy to generalize the obtained results to high-dimensional random inputs. Since the high-dimensional basis of gPC is constructed by tensor products of one-dimensional basis, the error of chaos expansion should be dominated by the summation of errors of one-dimensional truncation. Thus, the results for the one-dimensional case should be still valid for a high-dimensional case. For example, if we have d-dimensional uniform random inputs, ME-gPC with N^d uniform elements

should extend the valid integration time of gPC with the same polynomial order by a factor N. However, in practice, the degree of perturbation in each random dimension is generally different, and only the random dimensions with large perturbations are needed to be refined. Such cases are more difficult to analyze and beyond the scope of this paper.

3.5. Initial conditions

For the initial condition $u_0(x;\xi)$, we intentionally employed functions such as cosine and sine waves, which introduce "random periodicity" in time for a given random transport velocity. Such solutions are often encountered in practice, e.g., random oscillators and simulations of unsteady turbulent or noisy flows. If the frequency is finite, we know that the random solution can be expressed by a Fourier transform in the time direction

$$u(x,t;\xi) = \sum_{n=-M/2}^{M/2} u_n(x;\xi) e^{in\frac{2\pi}{T(\xi)}t}, \tag{48}$$

where $T(\xi)$ is the random period. It is obvious that Eq. (17) represents the basic properties of each random mode. We note that gPC can effectively capture the random behavior for some other initial conditions, e.g., $u_0(x;\xi) = x^n$, if the polynomial order is large enough.

The long-term behavior for aforementioned initial conditions is similar to the spectral expansion of deterministic functions with high wave numbers (see [24]). Since gPC is indeed a spectral expansion in terms of certain random variables and the time plays a role similar to a wave number in chaos expansion, the order of gPC must increase with time to maintain a desired accuracy level.

3.6. Numerical results

Next we present some numerical results for ϵ_M and $\hat{\epsilon}_M$. Let $n = 1$, $\bar{v} = 0$, $\sigma = 1$ in Eq. (16). Due to the periodic condition in physical space, we use a Fourier-collocation method to solve the deterministic PDEs introduced by the Galerkin projection in the gPC or ME-gPC method. It has been assumed that $q_M < 1$ for the convergence of summation in ϵ_M. However, q_M is an increasing function of t, which means that the error ϵ_M increases with time and it will reach O(1) values eventually. In Fig. 1, we present the evolution of the error bounds of gPC and ME-gPC, respectively. It can be seen that the error of ME-gPC increases at the same speed as that of gPC. However, since ME-gPC is much more accurate than gPC, it takes longer time for ME-gPC to reach O(1) error. The error ϵ_M of eighth-order gPC is O(1) around $t = 2$. In Fig. 2, ϵ_M and the corresponding numerical errors are shown, where we also plot $J^2_{i+1/2}(\sigma n\pi t)$ for comparison. It is known that $J^2_{i+1/2}(\sigma n\pi t)$ decreases exponentially with i when i is much greater than $\sigma n\pi t$; otherwise, there is no p-convergence. It can be seen that p-convergence does not occur until $M \geqslant 8$ ($q_M < 1$) and the rate of convergence is the same as the decreasing rate of $J^2_{i+1/2}(\sigma t\pi)$ when $i \to \infty$.

In Fig. 3 we demonstrate Theorem 5 numerically. According to Theorem 5, we know that the error of gPC at time t should be almost the same as the error of ME-gPC of the same polynomial order at time Nt for a uniform mesh. For gPC, we re-scale the time by a factor N while keeping the errors unchanged. It can be seen that the re-scaled error-time curve of gPC matches very well with the error-time curve of ME-gPC, and it appears that the errors of ME-gPC are always bounded by the shifted errors of gPC. We note that the random inputs are uniform.

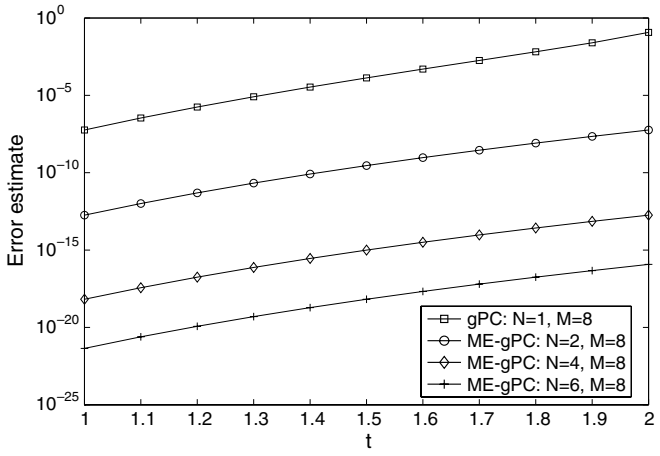

Fig. 1. Evolution of error estimates of gPC and ME-gPC. Here, ξ is uniform in $[-1,1]$.

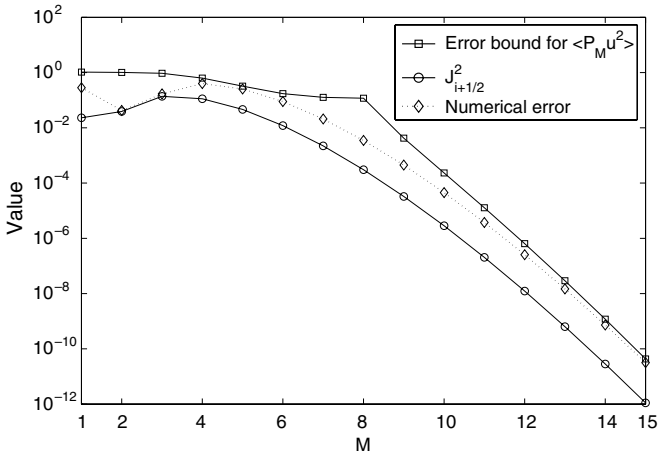

Fig. 2. Convergence of gPC and $J^2_{i+1/2}$ at $t = 2$. Here, ξ is uniform in $[-1, 1]$.

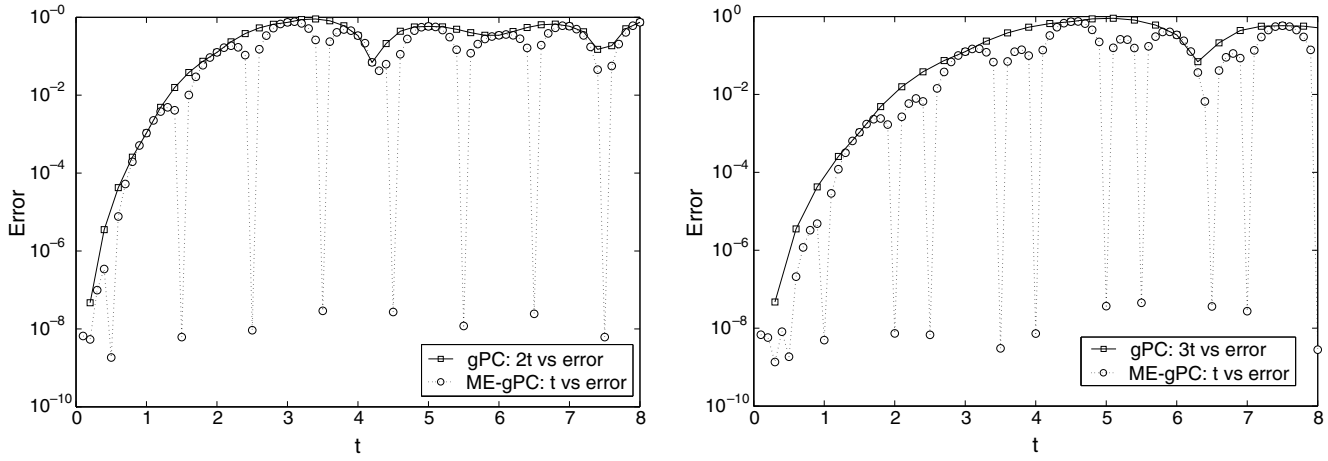

Fig. 3. Comparison of gPC and ME-gPC of the same polynomial order $p = 3$. Normalized numerical errors of the second moment are used. The time of gPC is multiplied by the number N of random elements. Here, ξ is of uniform distribution $U[-1, 1]$. Left: ME-gPC with $N = 2$; right: ME-gPC with $N = 3$.

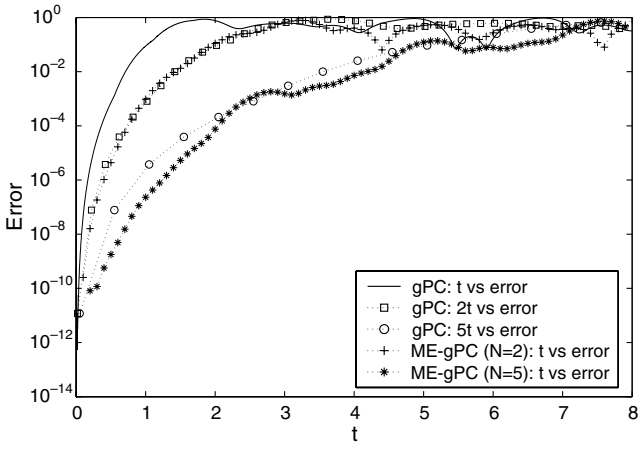

Fig. 4. Comparison of gPC and ME-gPC of the same polynomial order $p = 3$. Normalized numerical errors of the second moment are used. The time of gPC is multiplied by the number N of random elements. Here, ξ is of Beta distribution it Beta$(0, 1)$ on $[-1, 1]$.

To examine if the previous results extend to other random distributions, we consider Beta and Gaussian distributions. In Fig. 4, we plot the errors of gPC and ME-gPC versus time for a Beta distribution *Beta*$(0, 1)$ while the time for gPC is re-scaled as before. It is seen that the two curves for gPC and ME-gPC agree with each other very well. We also compare gPC

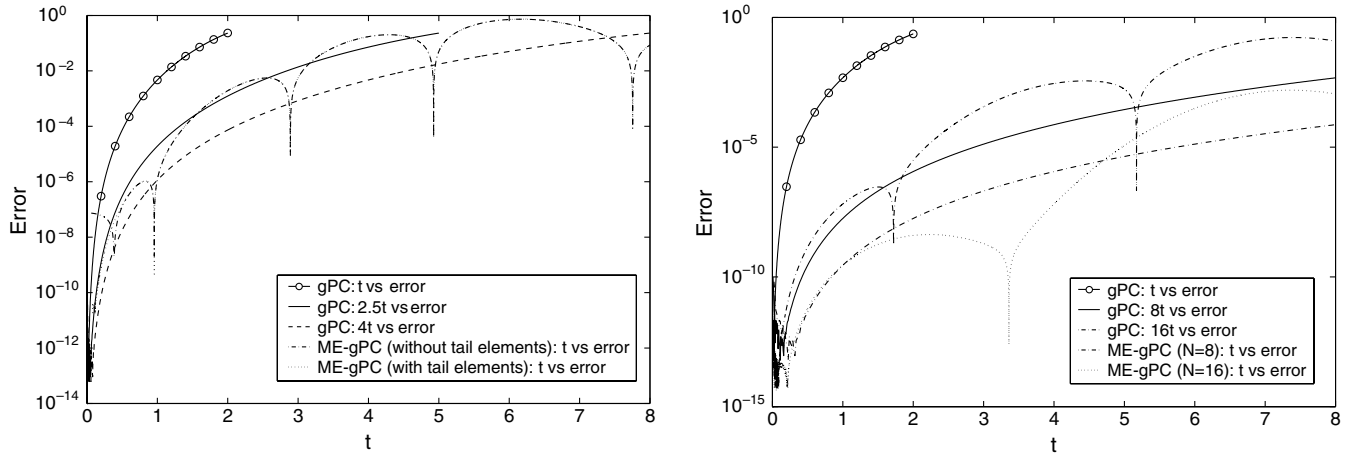

Fig. 5. Comparison of gPC and ME-gPC of the same polynomial order $p = 3$. Normalized numerical errors of the second moment are used. The time of gPC is re-scaled by a constant. Here, ξ is of Gaussian distribution $\mathcal{N}(0, 0.2)$. Left: ME-gPC with $N = 4$; right: ME-gPC with $N = 8, 16$.

and ME-gPC of polynomial order $p = 3$ in Fig. 5 when ξ is of Gaussian distribution. For the ME-gPC method, we first decompose the support of the Gaussian distribution into three random elements: $(-\infty, -6]$, $[-6, 6]$ and $[6, \infty)$. We subsequently decompose the middle element $[-6, 6]$ while keeping the tail elements unchanged since $\Pr(\xi \in (-\infty, -6]$ or $[6, \infty)) = 1.97 \times 10^{-9}$. The influence of tail elements can be observed only in the early stage, which is clearly shown in the left plot. Starting from $t \approx 0.5$, the tail elements will not affect the accuracy any more. Thus, we can drop the tail elements when we re-scale the error curves of gPC by the element number N due to their negligible error contribution. In the plot on the left, it can be seen that the error curve re-scaled by factor 2.5 matches the ME-gPC results better than the element number $N = 4$. The reason is that Gaussian distribution is non-uniform. If the middle element is decomposed to four equidistant ones, we know that $\Pr(I_{[-6,3]} = 1$ or $I_{[3,6]} = 1) = 2.7 \times 10^{-3}$, which implies that the error of ME-gPC is mainly controlled by elements $[-3, 0]$ and $[0, 3]$ (see Eq. (33)). Thus the scale factor should be about 2. In the plot on the right, we can see that for larger element numbers, the re-scaled error curves of gPC agree well with the ME-gPC results, which implies the relation presented in Theorem 5 will be valid asymptotically for the Gaussian distribution.

4. Application: noisy flow past a stationary circular cylinder

4.1. Random-frequency inflow noise

The aforementioned issues are often encountered in numerical simulations of unsteady noisy flows. We now simulate the two-dimensional noisy flow past a circular cylinder subject to the following random boundary conditions at the inflow

$$u = 1 + \sigma Y, \qquad v = 0, \tag{49}$$

where Y is a *uniform* random variable of zero mean and unit variance and σ is a prescribed constant indicating the degree of perturbation. For each value of Y, there exists a corresponding Reynolds number, which determines a unique vortex shedding frequency. In other words, the shedding frequency in the stochastic simulation is random.

In Fig. 6 the mesh used for the discretization in physical space is shown. Neumann boundary conditions (zero flux) are employed at the outflow and periodic boundary conditions in the cross-flow direction. The numerical formulation of gPC for the incompressible Navier–Stokes equations was presented in [25], where spectral/*hp* element methods were employed to solve the large deterministic PDE system produced by the Galerkin projection in gPC. The Reynolds number considered in this work is $Re = 100$.

We first simulate a deterministic case with $\sigma = 0$ up to $t = 1000$ to obtain a fully developed flow and then introduce 10% noise at the inflow. We plot the instantaneous mean and variance of lift coefficient C_L in Fig. 7, and of drag coefficient C_D in Fig. 8. It can be seen that both the mean and variance of C_L given by ME-gPC oscillate periodically around a constant value with a decreasing amplitude after a short transient stage. This agrees with a stochastic model of lift coefficient developed in [18,26], where C_L is modeled by a harmonic signal with a random frequency. Based on such a model, the mean of C_L goes to zero while the variance asymptotes a constant value. Good agreement between gPC and ME-gPC is observed only in the transient stage, after which gPC begins to diverge. Similar trends are observed for the drag coefficient C_D. The study in previous section shows that the polynomial order of gPC must increase at about a constant rate (see Eq. (38)) to maintain a certain accuracy if a random frequency is involved. In Fig. 9, we plot the normalized relative errors of the

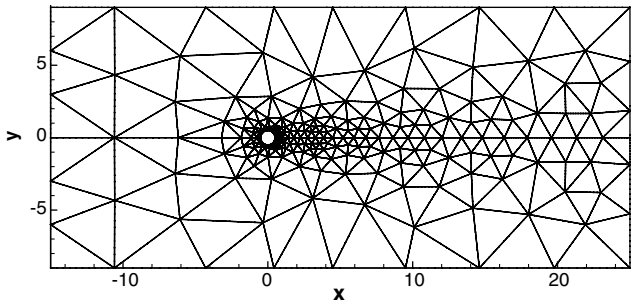

Fig. 6. Schematic of the domain for noisy flow past a circular cylinder. The size of the domain is $[-15D, 25D]\times[-9D, 9D]$ and the cylinder is at the origin with diameter $D = 1$. The mesh consists of 412 triangular elements.

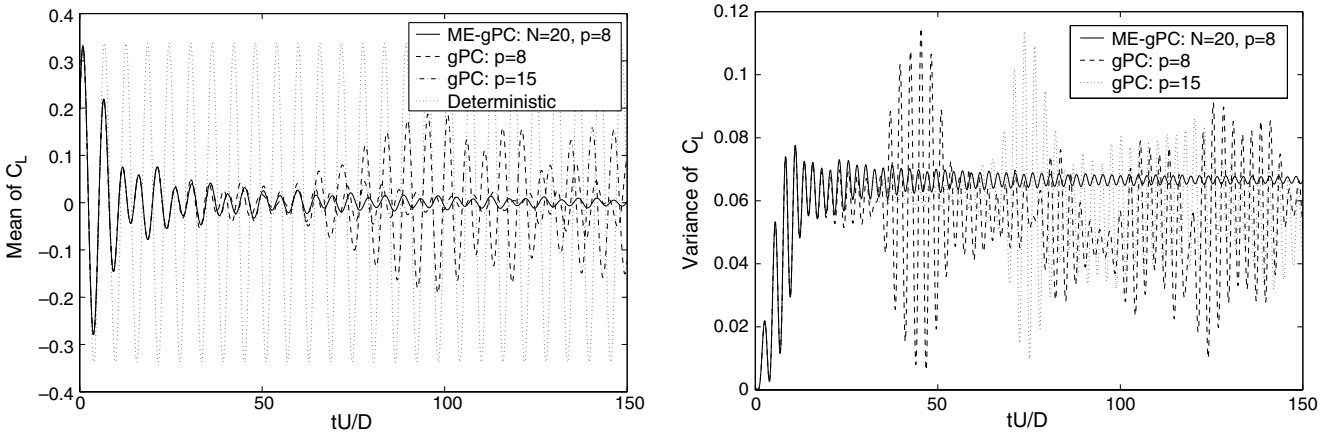

Fig. 7. Evolution of mean (left) and variance (right) of lift coefficient. Y is uniform in $[-\sqrt{3}, \sqrt{3}]$. $\sigma = 0.1$.

variance of the lift coefficient using the results given by ME-gPC with $N = 20$ and $M = 8$ as a reference. It can be seen that the errors of gPC increase quickly to O(1). ME-gPC with $N = 20$ and $p = 6$ reaches an error of $O(10^{-2})$ at $t \approx 135$. We note that errors less than 10^{-5} are not shown because the output data are truncated after the fifth digit.

In Section 3 we have shown that the error of ME-gPC at a fixed time can be estimated from that of gPC of the same polynomial order but shifted by a factor N. Here we cannot use this result directly because the decomposition of random shedding frequencies is not necessarily uniform although the noise at the inflow is uniform. However, we can estimate the scaling factor from the simulation results for the errors of gPC and ME-gPC of sixth order, which is about 12. Using this value we know that the error of ME-gPC with $N = 20$ and $M = 8$ at $tU/D = 150$ should be roughly equal to the error of eighth-order gPC at $tU/D = 150/12$, which is $O(10^{-3})$. Thus, ME-gPC with $N = 20$ and $M = 8$ can provide accurate results in the range $tU/D \leqslant 150$, corresponding to about 20 shedding periods after the transient stage. In contrast, gPC provides accurate result up to less than two shedding periods.

In Fig. 10 the RMS of vorticity is plotted. The global structure is (approximately) symmetric and the values of RMS of vorticity are decreasing gradually from the front stagnation point, through the boundary layers, into the wake. This suggests that the vorticity behind the cylinder should contain a harmonic signal $A(\mathbf{x}, Y)\cos(2\pi f_v(Y)t)$ with random frequencies f_v. The RMS of such a harmonic response will approach $\int_Y A^2(\mathbf{x}, Y)f(Y)/2\,\mathrm{d}Y$ as $t \to \infty$, where $f(Y)$ is the PDF of Y. Since the flux of vorticity decreases in the x direction due to viscous diffusion, the value of $A(\mathbf{x}, Y)$ should also decrease in the x direction. This explains qualitatively why we only observe decreasing RMS values of vorticity in the wake without the von Karmon vortex street.

4.2. Random-amplitude inflow noise

In this section we consider another noisy boundary condition at the inflow

$$u = 1 + \sigma\xi\cos 2\pi f_{\mathrm{in}}t, \qquad v = 0, \tag{50}$$

where we add a harmonic signal with a random amplitude into the inflow. We use $f_{\mathrm{in}} = 0.75f_s$, where f_s is the vortex shedding frequency at $Re = 100$. Let ξ be a uniform random variable with zero mean and unit variance. We set σ to 0.1.

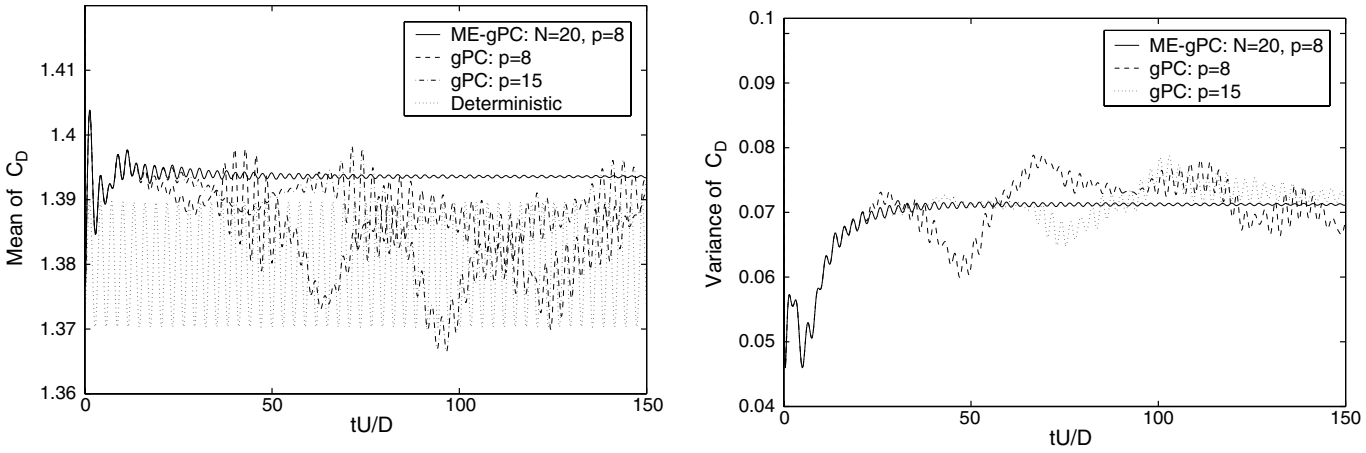

Fig. 8. Evolution of mean (left) and variance (right) of drag coefficient. Y is uniform in $[-\sqrt{3}, \sqrt{3}]$. $\sigma = 0.1$.

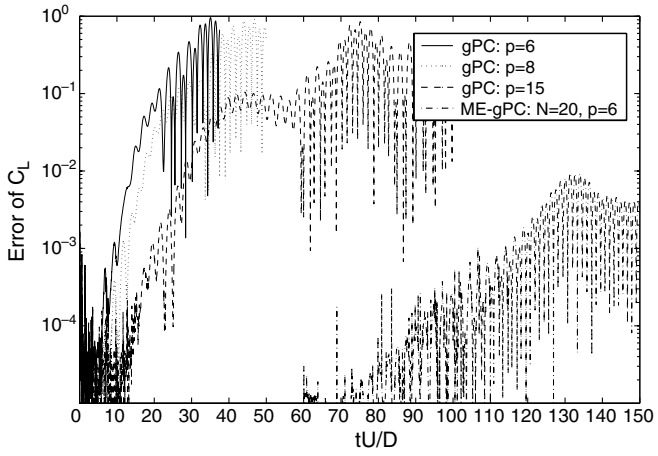

Fig. 9. Evolution of relative errors of instantaneous variance of lift coefficients given by gPC and ME-gPC. The results obtained from ME-gPC with $N = 20$ and $M = 8$ are used as a reference.

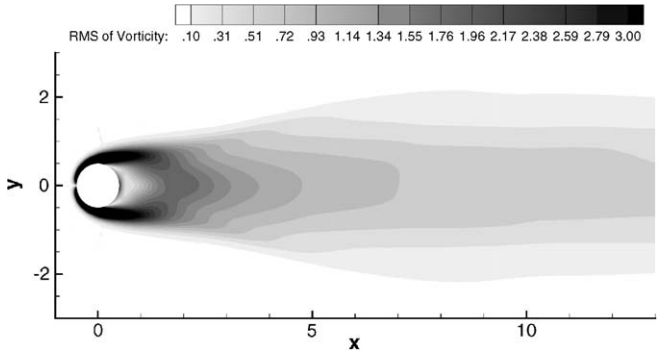

Fig. 10. Instantaneous spatial distribution of RMS of vorticity at $tU/D = 100$. $N = 20$ and $M = 8$.

In Fig. 11 we compare the mean and variance of C_L given by gPC and ME-gPC of the same order $M = 8$, where $N = 10$ for the ME-gPC. We see that eighth-order gPC can capture all the statistics up to the second-order in the range of $tU/D \leqslant 150$ in contrast to the fast divergence of gPC for the random-frequency noise. Numerical experiments show that for the boundary condition (50) the frequency of C_L is not sensitive to the boundary noise, where the vortex shedding frequency at $Re = 100$ is dominant. Thus, the error of gPC increases much slower than the first case. A similar example is noisy flow past an oscillating circular cylinder [4], where the frequency is also not sensitive to the noise and thus gPC

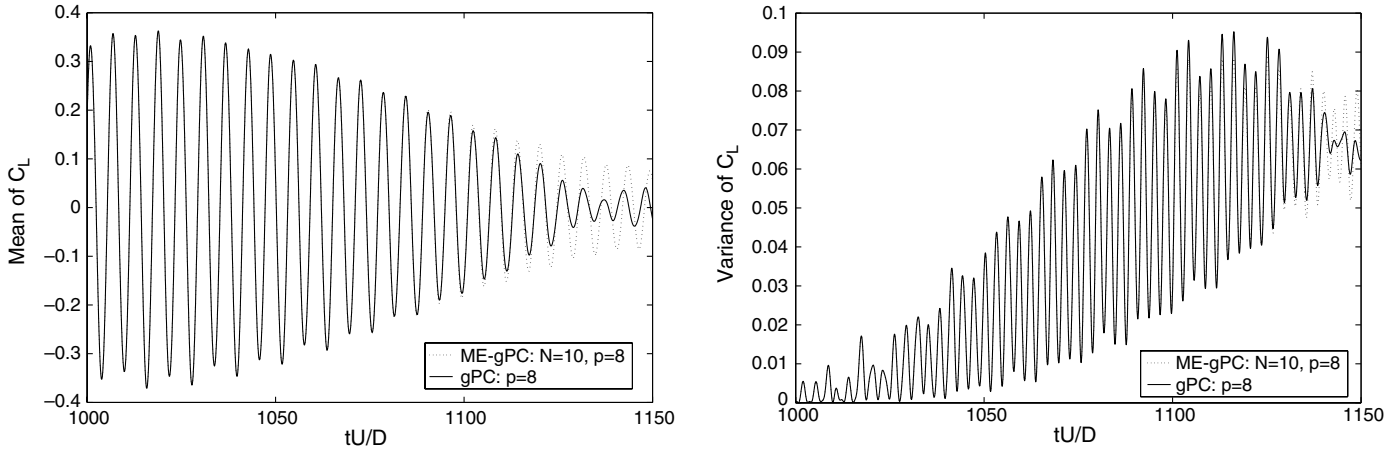

Fig. 11. Evolution of mean (left) and variance (right) of C_L given by gPC and ME-gPC. Here, ξ is a uniform random variable in $[-\sqrt{3}, \sqrt{3}]$ with $\sigma = 0.1$.

can do a good job. Such observations imply that the presence of random frequencies can cause a significant degradation of the performance of gPC, and thus employing ME-gPC is necessary for convergent results.

5. Summary

In this work we studied the long-term behavior of gPC and ME-gPC by focusing on problems related to random frequencies. We first analyzed the one-dimensional advection equation with a uniform random transport velocity, for which the error estimates of gPC and ME-gPC were derived for the Legendre-chaos expansion. Based on the error estimates, we found that ME-gPC with a uniform mesh in random space can *extend* the valid integration time of gPC by a factor N, which is the number of random elements. Subsequently, we extended this relation to other random distributions and verified it by numerical studies on Beta and Gaussian distributions. We then simulated noisy flow past a stationary circular cylinder, where two different boundary conditions at the inflow were considered. For the random-frequency noise at the inflow, the vortex shedding frequency is sensitive to the inflow condition; thus gPC fails to converge at early integration times but ME-gPC can capture the correct random behavior effectively. For the random-amplitude noise at the inflow, the shedding frequency is not as sensitive; thus gPC is valid for a relative longer time. This flow problem provides good support for our analysis in Section 3. Although ME-gPC can improve the performance of gPC for problems related to random frequencies, it also fails asymptotically. To treat this, one choice is to increase adaptively the number of elements of ME-gPC to maintain a reasonable accuracy in a desired range of integration time. However, for high-dimensional random inputs, the effectiveness of ME-gPC will be weakened since the number of elements may increase fast. Thus, the long-term behavior of polynomial chaos deserves further study.

Acknowledgements

We would to dedicate this work to the memory of John Argyris. This work was supported by NSF, ONR and AFOSR and computations were performed on the DoD and NSF supercomputing centers.

References

[1] R.G. Ghanem, P. Spanos, Stochastic Finite Elements: A Spectral Approach, Springer-Verlag, New York, 1991.
[2] R.G. Ghanem, J. Red-Horse, Propagation of uncertainty in complex physical systems using a stochastic finite elements approach, Physica D 133 (1999) 137–144.
[3] D. Xiu, G.E. Karniadakis, Modeling uncertainty in steady state diffusion problems via generalized polynomial chaos, Comput. Methods Appl. Math. Engrg. 191 (2002) 4927–4948.
[4] D. Lucor, G.E. Karniadakis, Noisy inflows cause a shedding-mode switching in flow past an oscillating cylinder, Phys. Rev. Lett. 92 (15) (2004) 154101.
[5] I. Babuška, P. Chatzipantelidis, On solving elliptic stochastic partial differential equations, Comput. Methods Appl. Mech. Engrg. 191 (2002) 4093–4122.
[6] P. Frauenfelder, C. Schwab, R.A. Todor, Finite elements for elliptic problems with stochastic coefficients, Comput. Methods Appl. Mech. Engrg. 194 (2005) 205–228.
[7] N. Wiener, The homogeneous chaos, Am. J. Math. 60 (1938) 897–936.
[8] R.G. Ghanem, Ingredients for a general purpose stochastic finite element formulation, Comput. Methods Appl. Mech. Engrg. 168 (1999) 19–34.

[9] R.G. Ghanem, Stochastic finite elements for heterogeneous media with multiple random non-Gaussian properties, ASCE J. Engrg. Mech. 125 (1) (1999) 26–40.
[10] D. Xiu, G.E. Karniadakis, The Wiener–Askey polynomial chaos for stochastic differential equations, SIAM J. Sci. Comput. 24 (2) (2002) 619–644.
[11] O.P.L. Maitre, H.N. Njam, R.G. Ghanem, O.M. Knio, Uncertainty propagation using Wiener–Haar expansions, J. Comput. Phys. 197 (2004) 28–57.
[12] O.P.L. Maitre, H.N. Njam, R.G. Ghanem, O.M. Knio, Multi-resolution analysis of Wiener-type uncertainty propagation schemes, J. Comput. Phys. 197 (2004) 502–531.
[13] M.K. Deb, I. Babuška, J.T. Oden, Solution of stochastic partial differential equations using Galerkin finite element techniques, Comput. Methods Appl. Mech. Engrg. 190 (2001) 6359–6372.
[14] I. Babuška, R. Tempone, G.E. Zouraris, Galerkin finite element approximations of stochastic elliptic differential equations, SIAM J. Numer. Anal. 42 (2) (2004) 800–825.
[15] G.E. Karniadakis, S.J. Sherwin, Spectral/*hp* Element Methods for CFD, second ed., Oxford University Press, 2005.
[16] C. Schwab, *p*- and *hp*-Finite Element Methods: Theory and Applications in Solid and Fluid Mechanics, Clarendon Press, Oxford, 1998.
[17] S.A. Orszag, L.R. Bissonnette, Dynamical properties of truncated Wiener–Hermite expansions, Phys. Fluids 10 (12) (1967) 2603–2613.
[18] D. Lucor, Generalized Polynomial Chaos: Applications to Random Oscillators and Flow-structure Interactions, Ph.D. thesis, Brown University, Division of Applied Mathematics, 2004.
[19] X. Wan, G.E. Karniadakis, An adaptive multi-element generalized polynomial chaos method for stochastic differential equations, J. Comput. Phys. 209 (2) (2005) 617–642.
[20] X. Wan, G.E. Karniadakis, Multi-element generalized polynomial chaos for arbitrary probability measures, SIAM J. Sci. Comput., in press.
[21] W. Gautschi, On generating orthogonal polynomials, SIAM J. Sci. Stat. Comput. 3 (3) (1982) 289–317.
[22] D. Gottlieb, S.A. Orszag, Numerical Analysis of Spectral Methods: Theory and Applications, SIAM, Philadelphia, PA, 1977.
[23] M. Abramowitz, I.A. Stegun, Handbook of Mathematical Functions, Dover, New York, 1970.
[24] M. Ainsworth, Dispersive and dissipative behaviour of high order discontinuous Galerkin finite element method, J. Comupt. Phys. 198 (2004) 106–130.
[25] D. Xiu, G.E. Karniadakis, Modeling uncertainty in flow simulations via generalized polynomial chaos, J. Comput. Phys. 187 (2003) 137–167.
[26] X. Wan, Multi-element Generalized Polynomial Chaos for Differential Equations with Random Inputs: Algorithms and Applications, Ph.D. thesis, Brown University, Division of Applied Mathematics (in preparation).